

NANO EXPRESS

Open Access

One-pot hydrothermal synthesis of Mn_3O_4 nanorods grown on Ni foam for high performance supercapacitor applications

Dongwei Li¹, Fanhui Meng¹, Xiuling Yan^{1,2}, Lishan Yang³, Hua Heng¹ and Ye Zhu^{1*}

Abstract

$\text{Mn}_3\text{O}_4/\text{Ni}$ foam composites were synthesized by a one-step hydrothermal method in an aqueous solution containing only $\text{Mn}(\text{NO}_3)_2$ and $\text{C}_6\text{H}_{12}\text{N}_4$. It was found that Mn_3O_4 nanorods with lengths of 2 to 3 μm and diameters of 100 nm distributed on Ni foam homogeneously. Detailed reaction time-dependent morphological and component evolution was studied to understand the growth process of Mn_3O_4 nanorods. As cathode material for supercapacitors, Mn_3O_4 nanorods/composite exhibited superior supercapacitor performances with high specific capacitance ($263 \text{ F} \cdot \text{g}^{-1}$ at $1 \text{ A} \cdot \text{g}^{-1}$), which was more than 10 times higher than that of the $\text{Mn}_3\text{O}_4/\text{Ni}$ plate. The enhanced supercapacitor performance was due to the porous architecture of the Ni foam which provides fast ion and electron transfer, large reaction surface area, and good conductivity.

Keywords: Manganese oxide; Ni foam; Nanorod; Hydrothermal synthesis; Supercapacitor

Background

Pseudocapacitors, based on reversible redox reactions at/near the surface of the electrode, represent one type of supercapacitors having the potential for high energy densities [1-3]. As is known, the excellent electrode should primarily meet the following key requirements: (1) a large number of electroactive sites, (2) high transport rates of both electrolyte ions and electrons, and (3) high electronic conductivity [4]. Among various pseudocapacitor electrode materials, RuO_2 has been extensively studied because of its ultrahigh theoretical capacitance ($2,000 \text{ F} \cdot \text{g}^{-1}$ in a wide potential window of 1.4 V), a nearly metallic electrical conductivity and excellent chemical stability [5]. However, RuO_2 has the drawbacks of high cost and toxicity. Therefore, extensive efforts have been made to search for alternative materials, such as Ni, Co, or Mn-based oxides/hydroxides [6-9]. Because the energy density of a supercapacitor is proportional to the square of the cell voltage, the energy density of Ni- and Co-related materials is limited by the narrow potential window [10].

Mn_3O_4 is a potentially interesting electrode material for electrolytic supercapacitors due to its low cost, non-toxicity, environmental compatibility, and intrinsically high capacity [11,12]. However, the capacitance property of Mn_3O_4 has been rarely investigated because of its poor electronic conductivity. A common strategy with poor electronic conductors is to combine them into composites with conducting substrates such as nanoporous gold, various carbon materials, and Ni foam [13,14]. Ni foam, as a commercial material with high electronic conductivity and a desirable three-dimensional (3D) structure is widely used as the electrode substrate material [15,16]. It would not only reduce the diffusion resistance of electrolytes but also provide a large surface area for loading active material. There have been some reports on the synthesis of Ni- and Co-based oxides/hydroxides on Ni foam [17-20]. However, there are very few reports on the fabrication of Mn-based oxides/hydroxides on Ni foam, except for the $\text{MnO}_2/\text{CNT}/\text{Ni}$ foam electrode [21,22]. To the best of our knowledge, one-pot hydrothermal synthesis of Mn_3O_4 nanorods structures on Ni foam has not been reported.

Here, we report facile direct synthesis of Mn_3O_4 nanorods on Ni foam with diameters of about 100 nm and lengths of 2 to 3 μm via one-pot hydrothermal process,

* Correspondence: zhuye@sdu.edu.cn

¹School of Chemistry and Chemical Engineering, Shandong University, Jinan 250100, China

Full list of author information is available at the end of the article

without any additional surfactant. The extraordinary redox activity of the $\text{Mn}_3\text{O}_4/\text{Ni}$ foam composite is demonstrated in terms of pseudocapacitive performance. The effect of reaction time on the crystal growth mechanism and supercapacitor performance of the $\text{Mn}_3\text{O}_4/\text{Ni}$ foam is well discussed.

Methods

Chemicals

Hexamethylene tetramine ($\text{C}_6\text{H}_{12}\text{N}_4$) and $\text{Mn}(\text{NO}_3)_2$ (50%) solution were purchased from Shanghai Chemical Reagent Company (Shanghai, China), while Ni foam ($5 \text{ g}/100 \text{ cm}^2$) was purchased from Changsha Liyuan New Material Co., Ltd. (Changsha, China). All reagents used in this experiment were of analytical grade without further purification. The Ni foam was immersed in concentrated hydrochloric acid for 10 min and then washed with acetone, ethanol, and distilled water several times before use.

Synthesis of samples

In a typical procedure, 3 mL $\text{Mn}(\text{NO}_3)_2$ (50%) solution and 2 g $\text{C}_6\text{H}_{12}\text{N}_4$ were dissolved in 17 mL distilled water. After vigorously stirring, the resulting solution and the pre-cleaned Ni foam were transferred into a Teflon-lined stainless autoclave. The autoclave was sealed at 120°C for 10 h and then cooled to room temperature naturally. The products were washed with distilled water several times, and finally dried in a vacuum desiccator at 50°C . The deposit weight of Mn_3O_4 was accurately determined by calculating the weight difference between the Ni foam coated with Mn_3O_4 after the hydrothermal process and the Ni foam before the hydrothermal process.

Characterization

The morphology of samples was characterized by scanning electron microscopy (SEM, JEOL JSM-6700 F, Akishima-shi, Japan) at an accelerating voltage of 10 kV. The obtained samples were characterized by X-ray powder diffraction (XRD) on a Bruker D8 advanced X-ray diffractometer (Madison, WI, USA) with Cu K α radiation ($\lambda = 1.5418 \text{ \AA}$) at a scan rate of $0.02^\circ \cdot \text{s}^{-1}$. Raman spectra were obtained using LabRAM HR UV/vis/near-IR spectrometer (Kyoto, Japan) with an argon-ion continuous-wave laser (514.5 nm) as the excitation source.

The electrochemical measurements were performed in a standard three-electrode cell on a CHI 760D potentiostat at room temperature, where 1 cm^2 ($1 \times 1 \text{ cm}$) of the obtained composite was used as the working electrode, a Pt plate was chosen as the counter electrode and a saturated calomel electrode (SCE) was selected as the reference electrode. A 4-M NaOH solution was used as the electrolyte.

Results and discussions

Component characterization

To examine the phase composition and structure of the samples, XRD analysis was carried out and the pattern is shown in Figure 1a. The as-prepared sample displays typical hausmannite Mn_3O_4 diffraction lines, which is in agreement with JCPDS card 18-0803. The peaks at around 44° and 52° are indexed to the Ni planes (111) and (200) of the Ni foam substrate, respectively. This result indicates that the utilized hydrothermal conditions are favorable for the formation of pure Mn_3O_4 . Moreover, the XRD peaks are relatively broad, indicating that the crystals constituting the products are small in size. Raman spectra can be used to gain more information about structure (Figure 1b). Consistent with the XRD data, the peak at 652.3 cm^{-1} corresponding to the crystalline Mn_3O_4 structure are clearly observed [23].

Morphology characterization

The photographs of the Ni foam (a) and the $\text{Mn}_3\text{O}_4/\text{Ni}$ foam composite (b) are shown in Figure 2. The Ni foam

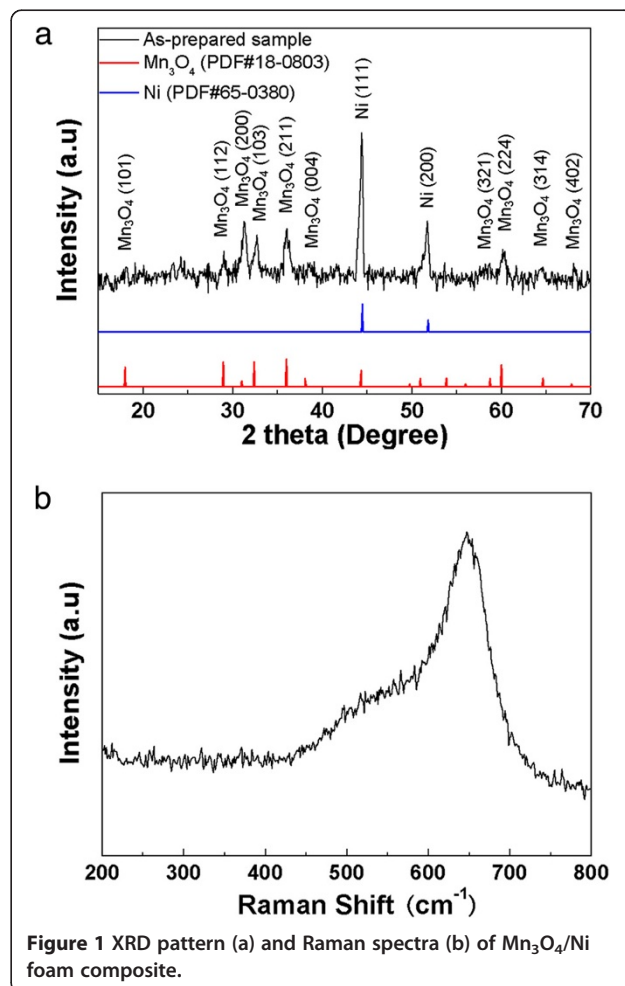


Figure 1 XRD pattern (a) and Raman spectra (b) of $\text{Mn}_3\text{O}_4/\text{Ni}$ foam composite.

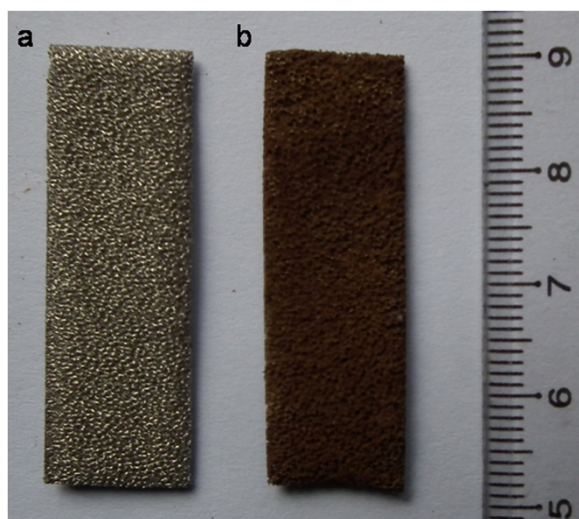


Figure 2 Digital photographs of (a) the Ni foam and (b) $\text{Mn}_3\text{O}_4/\text{Ni}$ foam composite.

turns to brown color after hydrothermal reaction, suggesting the formation of Mn_3O_4 on the Ni foam. The SEM image at low magnification shows that the pristine Ni foam has a 3D porous structure (Figure 3a). This porous skeleton of Ni foam would provide effective electrolyte accessible channels for ion transportation, and shorten the distance for ion diffusion. Figure 3b,c,d shows SEM images

of the $\text{Mn}_3\text{O}_4/\text{Ni}$ foam composite at different magnifications. These images show highly dense nanorods on Ni foam substrate. The individual nanorod is approximately 100 nm and approximately 2 to 3 μm in diameter and length, respectively, and the aspect ratio is greater than 20 in most cases.

Electrochemical capacitance of $\text{Mn}_3\text{O}_4/\text{Ni}$ foam electrode

Cyclic voltammetry (CV) and galvanostatic charging-discharging measurements were performed to evaluate the electrochemical properties and quantify the specific capacitance of the $\text{Mn}_3\text{O}_4/\text{Ni}$ foam composite. The CV curves of the composite at different scan rates between 5 and 20 $\text{mV} \cdot \text{s}^{-1}$ are presented in Figure 4a. Different from an ideal rectangular shape of the typical electrical double-layer capacitance, the redox reaction peaks indicate that the capacitance mainly results from the pseudocapacitive capacitance [24]. The pseudocapacitance arises from the reaction between the Mn^{4+} ions and NaOH electrolyte [25,26]. The peak current increases when the scan rate increases from 5 to 20 $\text{mV} \cdot \text{s}^{-1}$, while the anodic peaks shift toward the positive potential and cathodic peaks shift toward the negative potential, which demonstrates the quasi-reversible nature of the redox couples [27,28].

The charging-discharging curves of the $\text{Mn}_3\text{O}_4/\text{Ni}$ foam were measured at various current densities (shown in

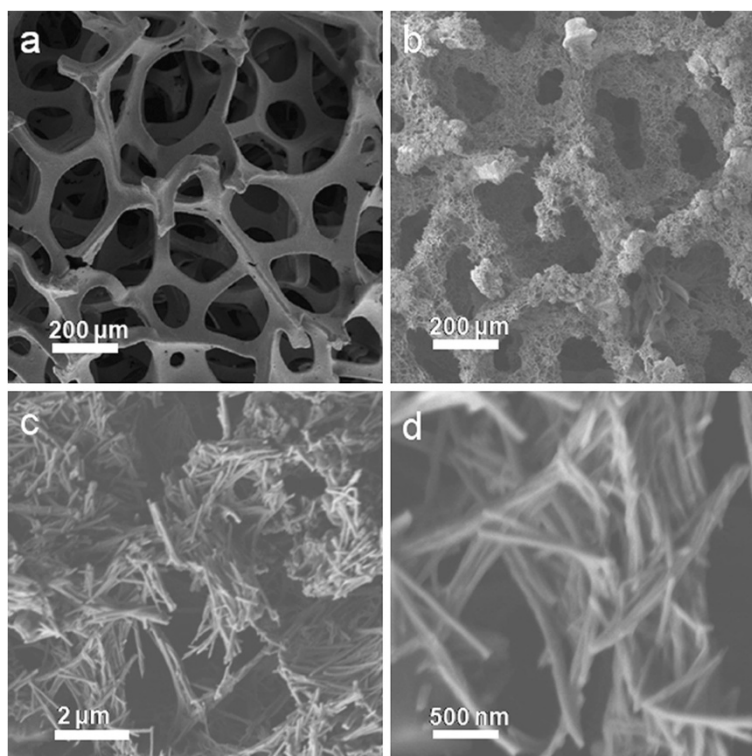


Figure 3 SEM images of (a) the 3D structure of Ni foam and (b,c,d) $\text{Mn}_3\text{O}_4/\text{Ni}$ foam composite with different magnifications.

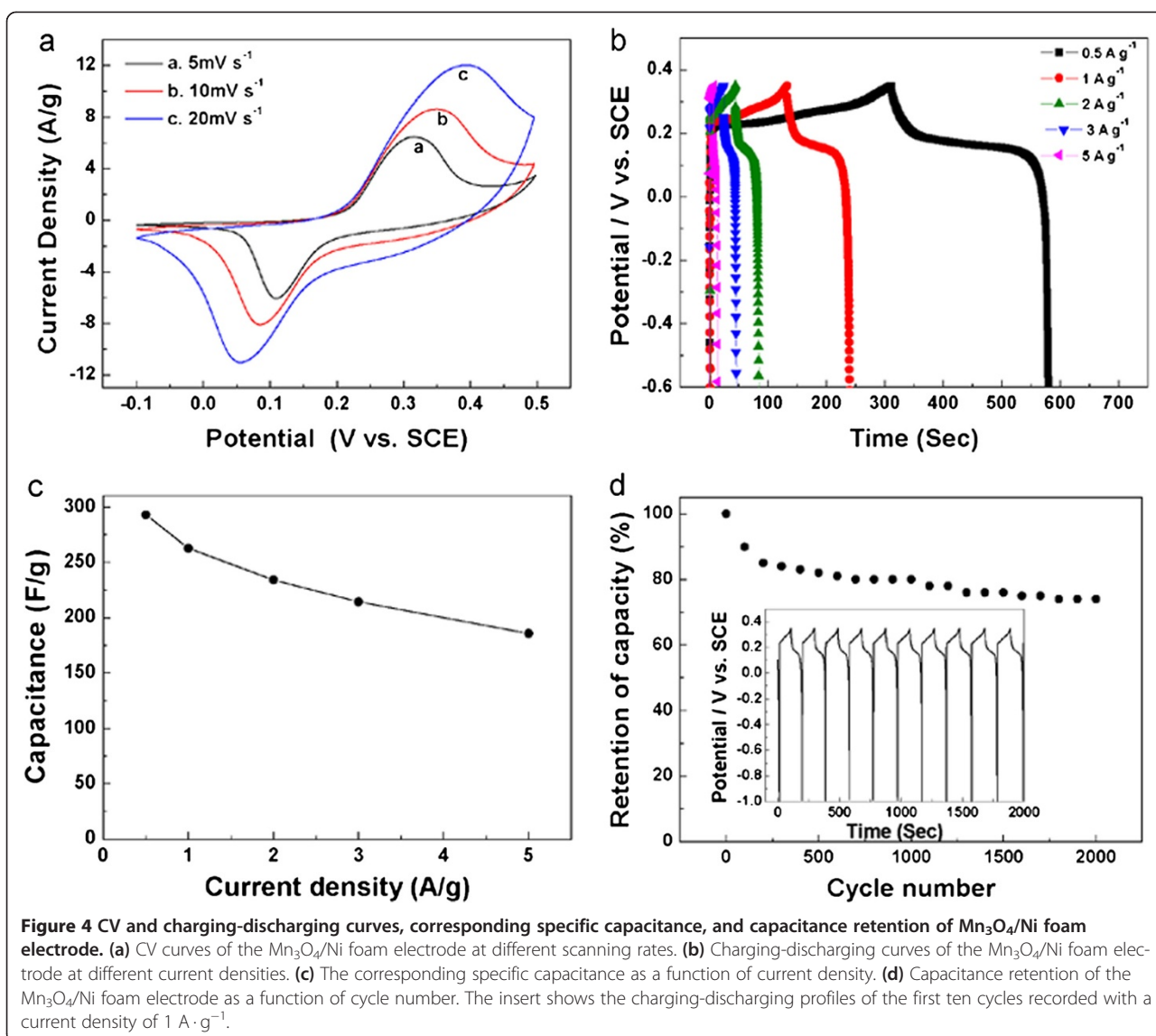


Figure 4b). The specific capacitance was calculated according to the following equation:

$$C = \frac{i \times \Delta t}{\Delta V}$$

where C (F g^{-1}) is the specific capacitance; i (A g^{-1}) is the discharge current density, Δt (s) is the discharge time, and ΔV (V) is the discharge potential range. The specific capacitance values of the $\text{Mn}_3\text{O}_4/\text{Ni}$ foam composite evaluated from the discharge curves are 293, 263, 234, 214, and 186 F g^{-1} at the current density of 0.5, 1, 2, 3, and 5 A g^{-1} , respectively (Figure 4c). The significant capacitance decrease with increasing discharge current density is likely to be caused by the increase of potential drop due to electrode resistance and the relatively insufficient Faradic redox reaction of the $\text{Mn}_3\text{O}_4/\text{Ni}$ foam composite under higher discharge current densities.

It is noteworthy that the specific capacitance of the as-prepared $\text{Mn}_3\text{O}_4/\text{Ni}$ foam composite is higher than of the previously reported Mn_3O_4 in other forms, i.e., Ma et al. reported a specific capacitance of 130 F g^{-1} (in $1 \text{ M Na}_2\text{SO}_4$ electrolyte at a current density of 1 A g^{-1}) for $\text{Mn}_3\text{O}_4/\text{graphene}$ nanocomposites prepared by a one-step solvothermal process [29], and Wang et al. reported a specific capacitance of 159 F g^{-1} (in 6 M KOH electrolyte at a scan rate of 5 mV s^{-1}) for $\text{Mn}_3\text{O}_4/\text{graphene}$ synthesized by mixing graphene suspension in ethylene glycol with MnO_2 organosol [30]. The high capacitance of the as-prepared $\text{Mn}_3\text{O}_4/\text{Ni}$ foam composite can be attributed to the positive synergistic effects between Mn_3O_4 and Ni foam. The skeleton of Ni foam could reduce the aggregation of the Mn_3O_4 nanorods, making the Mn_3O_4 nanorod accessible for electronic and ionic transport pathways and enhancing the utilization of the active materials.

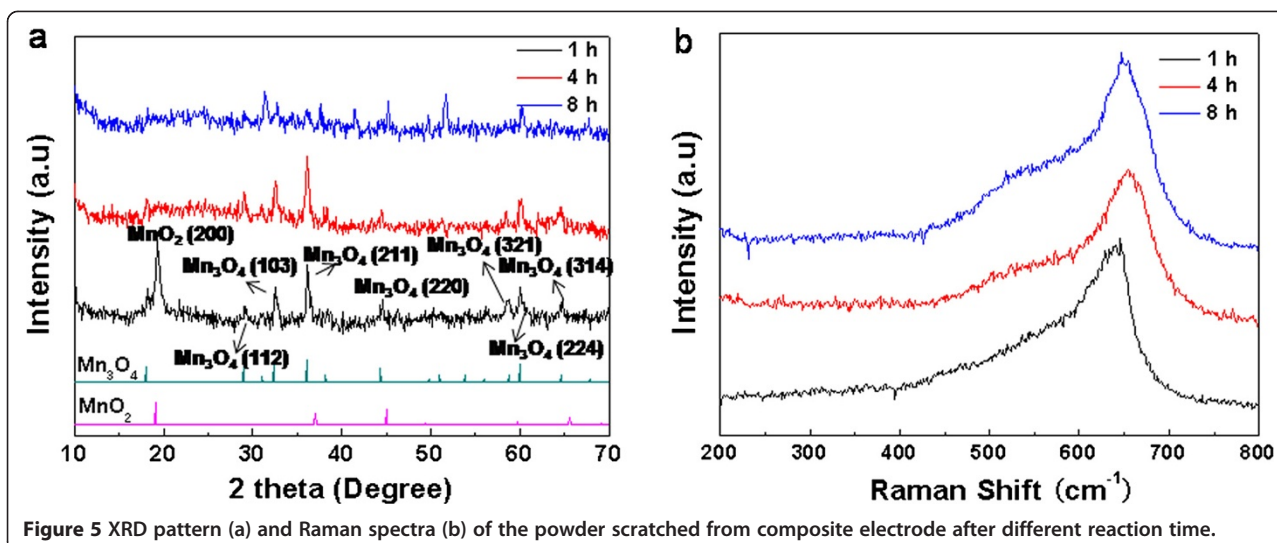


Figure 5 XRD pattern (a) and Raman spectra (b) of the powder scratched from composite electrode after different reaction time.

Furthermore, Ni foam also provides a highly conductive network for electron transport during the charge and discharge processes.

The endurance test was conducted using galvanostatic charging-discharging cycles at $1 \text{ A} \cdot \text{g}^{-1}$ (insert of Figure 4d). The discharge capacitance loss after 2,000 consecutive cycles is about 20%. The specific capacitance degradation is estimated to be from 263 to 205 $\text{F} \cdot \text{g}^{-1}$ (Figure 4d).

Although the Ni foam serves as a conductive matrix to promote fast Faradaic charging and discharging of the Mn₃O₄ nanorods, its loose structure leads to the flaking off of the nanorods from the Ni foam substrate.

Time-dependent Mn₃O₄/Ni foam composite properties

To shed light on the formation process, temporal evolution of the Mn₃O₄ nanostructures was studied by examining

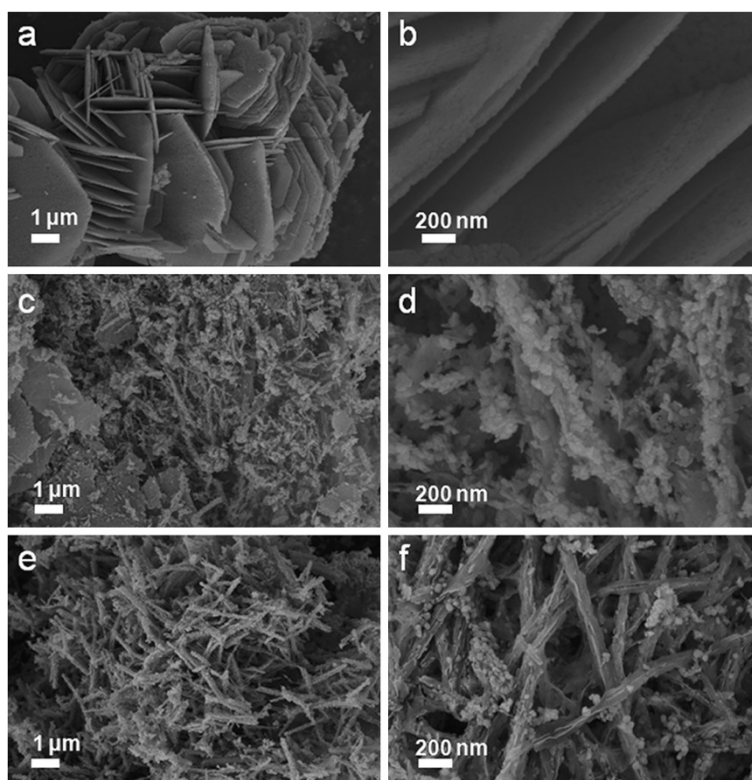
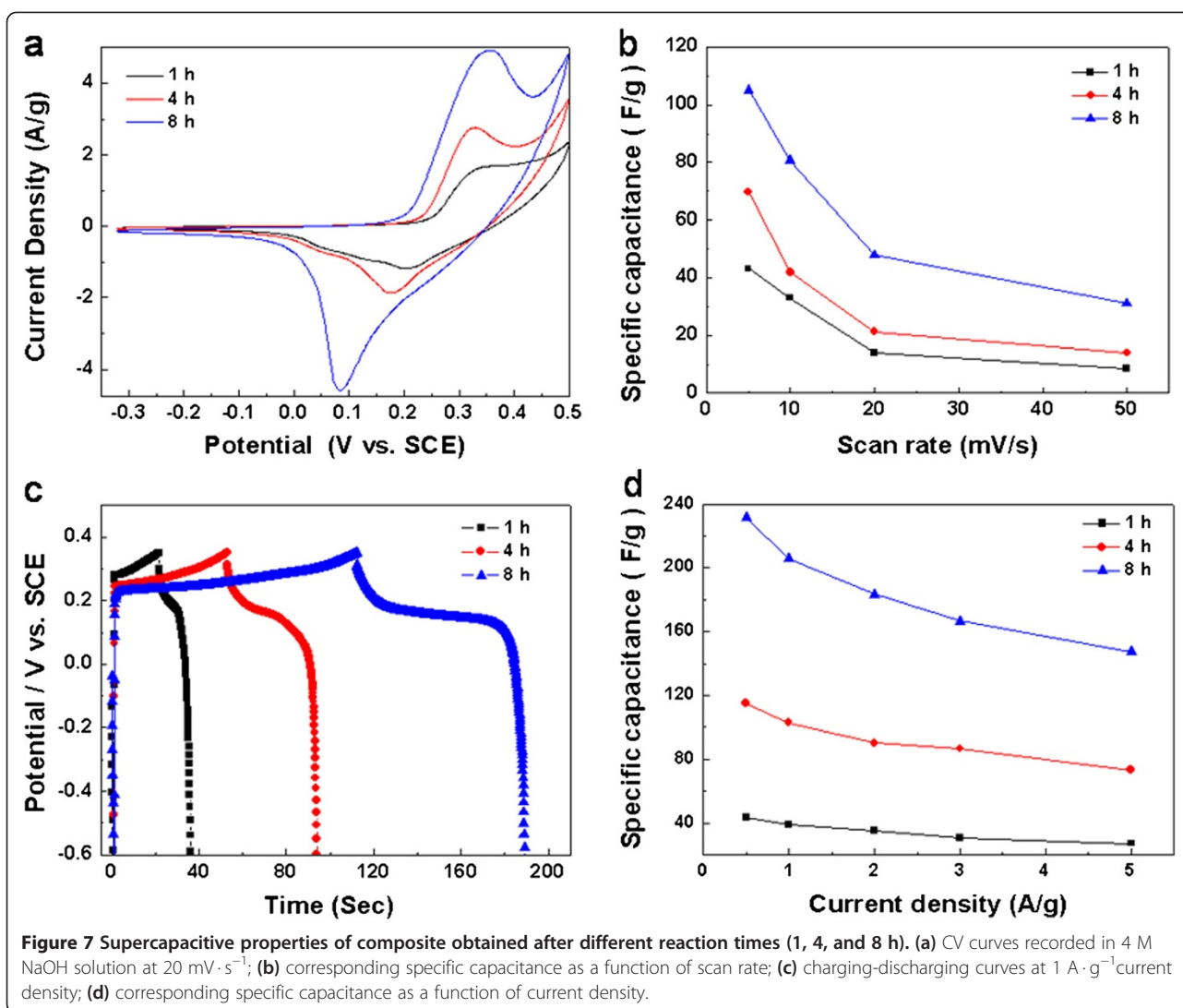


Figure 6 SEM images of composite obtained after different reaction times. (a,b) 1 h; (c,d) 4 h; (e,f) 8 h.



the products obtained under different reaction times of 1, 4, and 8 h. XRD patterns and Raman spectra were measured to identify the components of the different samples. The XRD patterns of the composite obtained under 1 h can be indexed to MnO_2 and Mn_3O_4 crystal structures (Figure 5a). For the composites obtained under 4 and 8 h, the intense XRD peak at $2\theta \approx 19^\circ$ disappeared corresponding to the MnO_2 (200) crystal structures and the left peaks attribute to the Mn_3O_4 crystal structures. Figure 5b shows the Raman spectra of the powder scratched from composite electrodes. The peak position of composites obtained under 4 and 8 h are red shifted compared with that of the composite obtained under 1 h. As is known, the Raman spectra for the MnO_2 phase and the Mn_3O_4 phase are located at 638.5 cm^{-1} and 652.5 cm^{-1} , respectively [31]. Therefore, this red shift of Raman spectra indicates the component variation from the MnO_2 phase to Mn_3O_4 , which is in excellent agreement with the result obtained from the XRD study. The SEM images of products

obtained under different reaction times of 1, 4, and 8 h are shown in Figure 6. The products collected after 1 h consisted of nanosheets with a thickness of about 30 nm (Figure 6a,b). When the reaction time increases to 4 h, some nanorods accompanied with nanoparticles begin to appear (Figure 6c,d). As the reaction proceeds to 8 h, the nanosheets disappeared and all of the products are nanorods with few nanoparticles (Figure 6e,f). After 10 h of the hydrothermal reaction, well-defined nanorods are obtained (Figure 3c,d). Based on the time-dependent morphology evolution described above, the formation mechanism of Mn_3O_4 nanorods can be proposed. At the initial stage, a large number of nanocrystallites nucleate and grow into nanosheets to minimize the overall energy of the system. However, the nanosheets are just intermediate products and not stable. After the reaction for 4 h, some of the nanosheets dissolve with the emergence of nanorods with some nanoparticles. When the reaction proceeds for 8 h, all of the nanosheets have transformed into nanorods with

nanoparticles. This suggests that the dissolution of nanosheets and the growth of nanorods occur simultaneously during the hydrothermal reaction. Further increase of the reaction time results in the development of well-defined and uniform nanorods without any impurity.

The electrochemical properties of products obtained under different reaction time were studied in 4 M NaOH solution. Figure 7a shows the CV curves of the products at a scan rate of $20 \text{ mV} \cdot \text{s}^{-1}$. As the reaction time increases from 1 to 8 h, the redox current density increases. The product obtained under 8 h may show the best capacitive behavior of the three products because the specific capacitance increases with the current density at the same scan rate. Figure 7b depicts the specific capacitance of the products under different reaction time at scan rates between 5 and $50 \text{ mV} \cdot \text{s}^{-1}$. All of them show that the specific capacitance gradually decreases as the scan rate increases, which can be attributed to the diffusion limitations in pore [22]. Obviously, the product obtained at 8 h has the highest specific capacitance, consistent with the CV tests in Figure 7a. The discharge curve of the composite obtained under 8 h displays a longer plateau than that of 1 and 4 h at $1 \text{ A} \cdot \text{g}^{-1}$ (Figure 7c). It is known that the increase of the charging time represents the higher capacitance at a fixed discharge current density. The dependence of the specific capacitance on the current density is compared in Figure 7d. The specific capacitance of the composite obtained at 1 h is 44, 39, 35, 31, and $27 \text{ F} \cdot \text{g}^{-1}$ at 0.5, 1, 2, 3, and $5 \text{ A} \cdot \text{g}^{-1}$, respectively. For current densities beyond $5 \text{ A} \cdot \text{g}^{-1}$, the iR drop is too large to permit an accurate calculation of the specific capacitance. In contrast, the specific capacitance of the composite obtained at 8 h is 232, 206, 183, 167, and $147 \text{ F} \cdot \text{g}^{-1}$ at the corresponding current densities. Combined with the curve in Figure 4b, the composite obtained at 10 h exhibits the highest specific capacitance. The increase in the specific capacitance can be attributed to the unique structure of the composite, and a longer period of reaction time leads to closer contact between the Ni foam substrate and the active material. Similar phenomena were also observed at the nanostructured $\text{Ni}(\text{OH})_2/\text{Ni}$ foam whose specific capacitance reached the highest after the longest reaction time [32].

Electrochemical capacitance of $\text{Mn}_3\text{O}_4/\text{Ni}$ plate electrode- comparison with $\text{Mn}_3\text{O}_4/\text{Ni}$ foam

As is known, the substrate is important to pseudocapacitor electrode materials. To investigate the electrochemical capacitance of the composite as a function of the substrate, control experiment was conducted using the Ni plate instead of the Ni foam for Mn_3O_4 growth under the same condition. Figure 8a shows the charging-discharging curves of the $\text{Mn}_3\text{O}_4/\text{Ni}$ plate measured at different current densities. Compared with the curve in

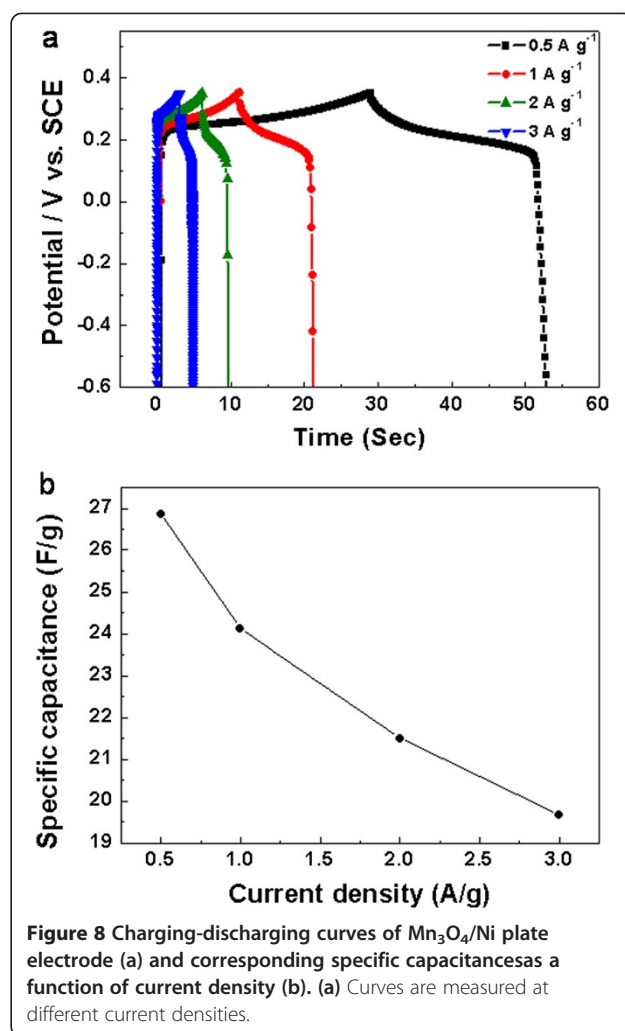


Figure 4b, the decrease in the charging time represents the lower capacitance of the $\text{Mn}_3\text{O}_4/\text{Ni}$ plate. The specific capacitances of the $\text{Mn}_3\text{O}_4/\text{Ni}$ plate are 27, 24, 21, and $19.6 \text{ F} \cdot \text{g}^{-1}$ at 0.5, 1, 2, and $3 \text{ A} \cdot \text{g}^{-1}$, respectively (Figure 8b). The specific capacitance of the $\text{Mn}_3\text{O}_4/\text{Ni}$ foam is more than 10 times higher than that of the $\text{Mn}_3\text{O}_4/\text{Ni}$ plate. The Ni foam substrate with microholes and zigzag flow channels results in excellent mass transport property and large surface area per unit volume of the electrode.

Conclusions

A facile one-step hydrothermal method was successfully developed to synthesize Mn_3O_4 nanorods on Ni foam. The complete absence of any surfactant enabled the product to have high purity. The formation process was proposed to include the dissolution of nanosheets, followed by the formation of uniform nanorods. The obtained Mn_3O_4 nanorods have diameters of about 100 nm and lengths of 2 to $3 \mu\text{m}$. A high specific capacitance of $263 \text{ F} \cdot \text{g}^{-1}$ has been achieved for the $\text{Mn}_3\text{O}_4/\text{Ni}$ foam at $1 \text{ A} \cdot \text{g}^{-1}$, which is

higher than that of the Mn_3O_4 composite on other substrates. Porosity may enhance the electrolyte/ Mn_3O_4 contact area and shorten the electrolyte diffusion length in the nanostructures. The cost-effective fabrication and remarkably high specific capacitance provide great potential for this type of hybrid nanostructure to be used as an active electrode for supercapacitor application.

Competing interests

The authors declare that they have no competing interests.

Authors' contributions

YZ and DL designed this research. DL carried out the experiments and analyzed the data. FM, XY, LY, and HH contributed to the discussion. DL and YZ wrote the paper. All authors read and approved the final manuscript.

Acknowledgements

This work was sponsored by the National Science Foundation of China (51171092), the Research Fund for the Doctoral Program of Higher Education of China (20090131110019) and the Independent Innovation Foundation of Shandong University (2012HW004).

Author details

¹School of Chemistry and Chemical Engineering, Shandong University, Jinan 250100, China. ²School of Chemistry and Bioscience, Ili Normal University, Xinjiang 835000, China. ³School of Chemistry and Chemical Engineering, Hunan Normal University, Changsha 410081, China.

Received: 12 November 2013 Accepted: 6 December 2013

Published: 19 December 2013

References

- Zhang JT, Zhao XS: On the configuration of supercapacitors for maximizing electrochemical performance. *Chem Sus Chem* 2012, **5**:818–841.
- Kim JH, Zhu K, Yan Y, Perkins CL, Frank AJ: Microstructure and pseudocapacitive properties of electrodes constructed of oriented NiO-TiO_2 nanotube arrays. *Nano Lett* 2010, **10**:4099–4104.
- Liu JP, Jiang J, Bosman M, Fan HJ: Three-dimensional tubular arrays of MnO_2 - NiO nanoplates with high areal pseudocapacitance. *J Mater Chem* 2012, **22**:2419–2426.
- Yuan CZ, Li JY, Hou LR, Zhang XG, Shen LF, Lou XW: Ultrathin mesoporous NiCo_2O_4 nanosheets supported on Ni foam as advanced electrodes for supercapacitors. *Adv Funct Mater* 2012, **22**:4592–4597.
- Zhao X, Sánchez BM, Dobson PJ, Grant PS: The role of nanomaterials in redox-based supercapacitors for next generation energy storage devices. *Nanoscale* 2011, **3**:839–855.
- Kim SI, Lee JS, Ahn HJ, Song HK, Jang JH: Facile route to an efficient NiO supercapacitor with a three-dimensional nanonetwork morphology. *ACS Appl Mater Interfaces* 2013, **5**:1596–1603.
- Wang HL, Casalongue HS, Liang YY, Dai HJ: Ni(OH)_2 nanoplates grown on graphene as advanced electrochemical pseudocapacitor materials. *J Am Chem Soc* 2010, **132**:7472–7477.
- Dong XC, Xu H, Wang XW, Huang YX, Chan-Park MB, Zhang H, Wang LH, Huang W, Chen P: 3D graphene-cobalt oxide electrode for high-performance supercapacitor and enzymeless glucose detection. *ACS Nano* 2012, **6**:3206–3213.
- Meng FH, Yan XL, Zhu Y, Si PC: Controllable synthesis of MnO_2 /polyaniline nanocomposite and its electrochemical capacitive property. *Nanoscale Res Lett* 2013, **8**:179.
- Lee GW, Hall AS, Kim J-D, Mallouk TE: A facile and template-free hydrothermal synthesis of Mn_3O_4 nanorods on graphene sheets for supercapacitor electrodes with long cycle stability. *Chem Mater* 2012, **24**:1158–1164.
- Xiao W, Xia H, Fuh JYH, Lu L: Growth of single-crystal α - MnO_2 nanotubes prepared by a hydrothermal route and their electrochemical properties. *J Power Sources* 2009, **193**:935–938.
- Dubal DP, Holze R: Self-assembly of stacked layers of Mn_3O_4 nanosheets using a scalable chemical strategy for enhanced, flexible, electrochemical energy storage. *J Power Sources* 2013, **238**:274–282.
- Meng FH, Ding Y: Sub-micrometer-thick all-solid-state supercapacitors with high power and energy densities. *Adv Mater* 2011, **23**:4098–4102.
- Zhang JT, Jiang JW, Zhao XS: Synthesis and capacitive properties of manganese oxide nanosheets dispersed on functionalized graphene sheets. *J Phys Chem C* 2011, **115**:6448–6454.
- Wang GL, Huang JC, Chen SL, Gao YY, Cao DX: Preparation and supercapacitance of CuO nanosheet arrays grown on nickel foam. *J Power Sources* 2011, **196**:5756–5760.
- Yu L, Zhang GQ, Yuan CZ, Lou XW: Hierarchical NiCo_2O_4 @ MnO_2 -core-shell heterostructured nanowire arrays on Ni foam as high-performance supercapacitor electrodes. *Chem Comm* 2013, **49**:137–139.
- Lu ZY, Chang Z, Liu JF, Sun XM: Stable ultrahigh specific capacitance of NiO nanorod arrays. *Nano Res* 2011, **4**:658–665.
- Yang GW, Xu CL, Li HL: Electrodeposited nickel hydroxide on nickel foam with ultrahigh capacitance. *Chem Comm* 2008:6537–6539.
- Guan C, Liu JP, Cheng CW, Li HX, Li XG, Zhou WW, Zhang H, Fan HJ: Hybrid structure of cobalt monoxide nanowire @ nickel hydroxide/nickel nanoplate aligned on nickel foam for high-rate supercapacitor. *Energ Environ Sci* 2011, **4**:4496–4499.
- Xia XH, Tu JP, Zhang YQ, Mai YJ, Wang XL, Gu CD, Zhao XB: Three-dimensional porous Ni-Co(OH)_2 nanoplate composite film: a pseudocapacitive material with superior performance. *J Phys Chem C* 2011, **115**:22662–22668.
- Zhao DD, Yang Z, Zhang LY, Feng XL, Zhang YF: Electrodeposited manganese oxide on nickel foam-supported carbon nanotubes for electrode of supercapacitors. *Electrochem Solid-State Lett* 2011, **14**:93–96.
- Li J, Yang QM, Zhitomirsky I: Nickel foam-based manganese dioxide-carbon nanotube composite electrodes for electrochemical supercapacitors. *J Power Sources* 2008, **185**:1569–1574.
- Wang WZ, Ao L: Synthesis and optical properties of Mn_3O_4 nanowires by decomposing MnCO_3 nanoparticles in flux. *Cryst Growth Des* 2008, **8**:358–362.
- Chen J, Huang KL, Liu SQ: Insoluble metal hexacyanoferrates as supercapacitor electrodes. *Electrochem Commun* 2008, **10**:1851–1855.
- Wang DW, Li YQ, Wang QH, Wang TM: Facile synthesis of porous Mn_3O_4 nanocrystal-graphene nanocomposites for electrochemical supercapacitors. *Eur J Inorg Chem* 2012, **2012**:628–635.
- Wei WF, Cui XW, Chen WX, Ivey DG: Manganese oxide-based materials as electrochemical supercapacitor electrodes. *Chem Soc Rev* 2011, **40**:1697–1721.
- Kong LB, Lang JW, Liu M, Luo YC, Kang L: Facile approach to prepare loose-packed cobalt hydroxide nano-plates materials for electrochemical capacitors. *J Power Sources* 2009, **194**:1194–1201.
- Qing XX, Liu SQ, Huang KL, Lv K, Yang YP, Lu ZG, Fang D, Liang XX: Facile synthesis of Co_3O_4 nanoflowers grown on Ni foam with superior electrochemical performance. *Electrochim Acta* 2011, **56**:4985–4991.
- Zhang X, Sun XZ, Chen Y, Zhang DC, Ma YW: One-step solvothermal synthesis of graphene/ Mn_3O_4 nanocomposites and their electrochemical properties for supercapacitors. *Mater Lett* 2012, **68**:336–339.
- Wang B, Park J, Wang CY, Ahn H, Wang GX: Mn_3O_4 nanoparticles embedded into graphene nanosheets: preparation, characterization, and electrochemical properties for supercapacitors. *Electrochim Acta* 2010, **55**:6812–6817.
- Xue ZH, Liu ZL, Ma FW, Sun LP, Huo LH, Zhao H: Hydrothermal synthesis of α - MnO_2 nanorods and their electrochemical performances. *Chin J Inorg Chem* 2012, **28**:691–697.
- Lv S, Suo H, Wang JM, Wang Y, Zhao C, Xing SX: Facile synthesis of nanostructured Ni(OH)_2 on nickel foam and its electrochemical property. *Colloid Surface Physicochem Eng Aspect* 2012, **396**:292–298.

doi:10.1186/1556-276X-8-535

Cite this article as: Li et al.: One-pot hydrothermal synthesis of Mn_3O_4 nanorods grown on Ni foam for high performance supercapacitor applications. *Nanoscale Research Letters* 2013 **8**:535.